Pobrane z czasopisma Annales AI- Informatica http://ai.annales.umcs.pl

Data: 06/09/2025 01:51:48



Annales UMCS Informatica AI 2 (2004) 283-290

Annales UMCS
Informatica
Lublin-Polonia
Sectio AI

http://www.annales.umcs.lublin.pl/

## A numerical model of MHD waves

Krzysztof Murawski\*, Małgorzata Selwa

Institute of Physics, Maria Curie-Skłodowska University, Radziszewskiego 10, 20-031 Lublin, Poland

#### Abstract

This paper is primarily concerned with a numerical model of MHD waves. While a hyperbolic system of wave equations admits a shock solution the MHD equations are not strictly hyperbolic. As a consequence of that these equations require special numerical treatment. An application of a resulting numerical code to a problem of wave propagation in a coronal loop is presented.

### 1. Introduction

Plasma reveals either fluid-like or particle-like behavior. In the magnetohydrodynamic (MHD) model, the plasma is treated like a conducting fluid having macroscopic parameters that accurately describe its particle-like interactions. This model combines fluid equations and Maxwell's equations [1].

Although the MHD theory is the simplest self-consistent model describing the macroscopic behavior of the plasma, the full nonlinear equations are so complex that usually several simplifications are necessary to yield tractable problems. Therefore, many solutions require numerical treatment. However, a principal difficulty associated with developing a numerical method for the MHD equations is that the MHD equations contain the magnetic field which has to satisfy the divergence-free constraint,  $\nabla \cdot \mathbf{B} = 0$ . A local nonzero divergence of magnetic field indicates the existence of magnetic monopoles within the numerical cell, which leads to nonconservation of the magnetic flux across its surface. Accumulation of the numerical errors associated with evolving the magnetic field components can lead to violation of this constraint, causing an artificial force parallel to the magnetic field, and eventually can force termination of the simulations. This has a considerable impact on a performance of the algorithms which are required to provide the stable and accurate fulfilment of the divergence-free constraint.

<sup>\*</sup> Corresponding author: e-mail address: kamur@tytan.umcs.lublin.pl

Despite the problems many numerical schemes have been developed for the MHD equations. These schemes reveal either conservative or non-conservative properties of the equations and they are briefly described in this paper as well as their performance for coronal loop waves.

### 2. General considerations

We consider a hyperbolic system of one-dimensional equations, which are written in the following form:

$$\mathbf{q}_{t} + \mathbf{f}_{x} = 0. \tag{1}$$

Here the state vector is  $\mathbf{q}$  and the flux vector  $\mathbf{f}$  are cell averaged quantities and the comma denotes partial differentiation, e.g.  $\mathbf{q}_{,t} = \frac{\partial \mathbf{q}}{\partial t}$ . Application of the chain rule to the derivative of the flux  $\mathbf{f}_{,x}$  gives a quasi-linear form of Eq. (1)

$$\mathbf{q}_{x} + \mathbf{A}\mathbf{q}_{x} = 0, \tag{2}$$

where  $\mathbf{A} = \mathbf{f}_{,\mathbf{q}}$  is the Jacobian matrix, whose elements are given by  $A_{ij} = f_{i,q_j}$ . We assume that  $\mathbf{A}$  is locally (inside each numerical cell) constant and consequently, this equation is referred to as the "locally frozen".

We discretize Eq. (1) with the use of the forward Euler schemes so that [2]

$$\mathbf{q}_{i}^{n+1} = \mathbf{q}_{i}^{n} - \frac{\Delta t}{\Delta x} \left( \mathbf{f}_{i+1/2}^{n} - \mathbf{f}_{i-1/2}^{n} \right), \tag{3}$$

where  $\mathbf{f}_{i+1/2}^n$  is the value of the numerical flux evaluated at interface i + 1/2 at time step n.

The procedure for constructing a numerical flux  $\mathbf{f}_{i+1/2}^n$  is to combine a high order flux  $\mathbf{f}^l$  with a low order flux  $\mathbf{f}^l$  such that

$$\mathbf{f}^h = \mathbf{f}^l + \left(\mathbf{f}^h - \mathbf{f}^l\right),\tag{4}$$

where the correction is the term in the braces. The magnitude of this correction is limited depending on the smoothness of the data. That is

$$\mathbf{f} = \mathbf{f}^l + \phi \left( \mathbf{f}^h - \mathbf{f}^l \right). \tag{5}$$

Here  $\phi$  is the flux limiter whose role is to switch smoothly the scheme between high and low accuracy. In the regions of space where this solution is smooth (large-gradients)  $\phi \approx 1(\phi = 0)$  and the scheme has high (low) accuracy.

The choice of the low order flux  $\mathbf{f}'$  is upwind scheme for which

$$\mathbf{f}_{i+1/2}^{l} = \frac{1}{2} \left( \mathbf{f}_{i} + \mathbf{f}_{i+1} \right) - \frac{1}{2} \operatorname{sgn} \left( \mathbf{\Lambda}_{i+1/2} \right) \left( \mathbf{f}_{i+1} - \mathbf{f}_{i} \right), \tag{6}$$

where  $\Lambda_{i+1/2}$  is a diagonal matrix with the elements equal to the eigenvalues of the flux Jacobian  $\mathbf{A}_{i+1/2} = (\mathbf{R}\Lambda\mathbf{L})_{i+1/2}$ , where  $\mathbf{R}$  and  $\mathbf{L} = \mathbf{R}^{-1}$  are matrices of the right and left eigenvectors. The flux difference can be expressed as [3]

$$\mathbf{f}_{i+1} - \mathbf{f}_i = \mathbf{A}_{i+1/2} \left( \mathbf{q}_{i+1} - \mathbf{q}_i \right) \tag{7}$$

from Eq. (6) we get

$$\mathbf{f}_{i+1/2}^{l} = \frac{1}{2} \left( \mathbf{f}_{i} + \mathbf{f}_{i+1} \right) - \frac{1}{2} \left( \mathbf{R} \left| \mathbf{\Lambda} \right| \mathbf{L} \right)_{i+1/2} \left( \mathbf{q}_{i+1} - \mathbf{q}_{i} \right). \tag{8}$$

This equation can be simplified by noticing that the strength of the m-th wave is expressed by the dot-product of the left eigenvector  $\mathbf{l}^m$  and the jump of the conserved variables across the interface

$$\alpha_{i+1/2}^m = \mathbf{l}^m \cdot (\mathbf{q}_{i+1} - \mathbf{q}_i). \tag{9}$$

We obtain then

$$\mathbf{f}_{i+1/2}^{l} = \frac{1}{2} (\mathbf{f}_{i} + \mathbf{f}_{i+1}) - \frac{1}{2} \sum_{m} (|\lambda^{m}| \alpha^{m} \mathbf{r}^{m})_{i+1/2}.$$
 (10)

This first order accurate upwind flux is used in the neighborhood of steep profiles in order to suppress induced oscillations numerically. Second order accurate fluxes are achieved by using a flux limiter that modifies the first order flux so that it uses second order differencing in smooth portions of the flow [4].

# 3. Non-conservative equations

The original MHD equations can be written in the quasilinear form of Eq. (2) in which  $\mathbf{q} = (\rho, \rho \mathbf{v}, \mathbf{B}, p)^T$  and

$$\mathbf{A} = (\rho, \rho \mathbf{v}, \mathbf{B}, p) \text{ and}$$

$$\begin{pmatrix} v_x & \rho & 0 & 0 & 0 & 0 & 0 & 0 \\ 0 & v_x & 0 & 0 & -\frac{B_x}{\rho} & \frac{B_y}{\rho} & \frac{B_z}{\rho} & \frac{1}{\rho} \\ 0 & 0 & v_x & 0 & -\frac{B_y}{\rho} & -\frac{B_x}{\rho} & 0 & 0 \\ 0 & 0 & 0 & v_x & -\frac{B_z}{\rho} & 0 & -\frac{B_x}{\rho} & 0 \\ 0 & 0 & 0 & 0 & 0 & 0 & 0 & 0 \\ 0 & B_y & -B_x & 0 & -v_y & v_x & 0 & 0 \\ 0 & B_z & 0 & -B_x & -v_z & 0 & v_x & 0 \\ 0 & \gamma p & 0 & 0 & (\gamma - 1) \mathbf{v} \cdot \mathbf{B} & 0 & 0 & v_x \end{pmatrix}$$

$$(11)$$

It is noteworthy that the 5-th row from the top of the matrix **A** consists of zeroes. This is a consequence of the fact that  $(\nabla \cdot \mathbf{B})_{,t} = 0$ . As a result of the zero row, we find that the 8-th eigenvalue of **A**\$ is zero, *i. e.* 

$$w^{8}_{,t} + 0w^{8}_{,x} = 0, (12)$$

where  $w^8 = B_r$ .

3

The MHD equations can be also written in the non-conservative form

$$\mathbf{q}_{t} + \mathbf{f}_{x} = -B_{x,x} (0, \mathbf{B}, \mathbf{v}, \mathbf{v} \cdot \mathbf{B})^{T}, \quad B_{x,x} = 0$$
(13)

or in its quasi-linear counterpart

where A is the matrix defined by Eq. (11). This equation can be rewritten in the quasilinear form of Eq. (2) with

$$\mathbf{A} = \begin{pmatrix} v_{x} & \rho & 0 & 0 & 0 & 0 & 0 & 0 \\ 0 & v_{x} & 0 & 0 & 0 & \frac{B_{y}}{\rho} & \frac{B_{z}}{\rho} & \frac{1}{\rho} \\ 0 & 0 & v_{x} & 0 & 0 & -\frac{B_{x}}{\rho} & 0 & 0 \\ 0 & 0 & 0 & v_{x} & 0 & 0 & -\frac{B_{x}}{\rho} & 0 \\ 0 & 0 & 0 & 0 & 0 & 0 & 0 & 0 \\ 0 & B_{y} & -B_{x} & 0 & 0 & v_{x} & 0 & 0 \\ 0 & B_{z} & 0 & -B_{x} & 0 & 0 & v_{x} & 0 \\ 0 & \gamma p & 0 & 0 & 0 & 0 & 0 & v_{x} \end{pmatrix}.$$

$$(15)$$

So, we see that the zero row has disappeared and the eight wave now satisfies the advection equation

$$w_{t}^{8} + v_{x}w_{x}^{8} = 0. {16}$$

As this wave carries non-zero magnetic field divergence it is nicknamed the divergence wave.

## 4. Eigenvalues and eigenvectors

The Jacobian matrix  $\overline{\mathbf{A}}$  has the eigenvalues ( $\lambda$ ) and left ( $\mathbf{l}$ ) and right ( $\mathbf{r}$ ) eigenvectors which correspond to the following waves [5]:

Four magnetosonic waves with:

$$\mathbf{I}^{\pm} = V_{x} \pm c_{\pm}, \qquad (17)$$

$$\begin{pmatrix}
0 \\
\pm \rho c_{\pm} \\
\mp \frac{B_{x}B_{y}\rho c_{\pm}}{\rho c_{\pm}^{2} - B_{x}^{2}} \\
\mp \frac{B_{x}B_{z}\rho c_{\pm}}{\rho c_{\pm}^{2} - B_{x}^{2}} \\
0 \\
\frac{B_{y}\rho c_{\pm}}{\rho c_{\pm}^{2} - B_{x}^{2}} \\
\frac{B_{z}\rho c_{\pm}}{\rho c_{\pm}^{2} - B_{x}^{2}}
\end{pmatrix}$$

$$\mathbf{r}^{\pm} = N^{\pm}$$

$$\begin{pmatrix}
\rho \\
\pm c_{\pm} \\
\mp \frac{B_{x}B_{y}c_{\pm}}{\rho c_{\pm}^{2} - B_{x}^{2}} \\
0 \\
\frac{B_{y}\rho c_{\pm}^{2}}{\rho c_{\pm}^{2} - B_{x}^{2}} \\
\frac{B_{z}\rho c_{\pm}^{2}}{\rho c_{\pm}^{2} - B_{x}^{2}}
\end{pmatrix}$$

$$\frac{B_{z}\rho c_{\pm}}{\rho c_{\pm}^{2} - B_{x}^{2}}$$

$$\frac{B_{z}\rho c_{\pm}^{2}}{\rho c_{\pm}^{2} - B_{x}^{2}}$$

$$\frac{B_{z}\rho c_{\pm}^{2}}{\rho c_{\pm}^{2} - B_{x}^{2}}$$

where  $N^{\pm}$  stands for a normalization factor such that  $\mathbf{l}^{\pm}\mathbf{r}^{\pm}=1$ . This factor is too complicated to be printed here. The superscript  $\pm$  corresponds to the fast  $(c_{+})$  and slow  $(c_{-})$  magnetosonic wave speeds.

Two Alfvén waves with:

$$\lambda^a = \nu_x \pm V_A \,, \tag{19}$$

$$\mathbf{l}^{a} = \frac{1}{2\sqrt{N}} \left( 0, 0, -B_{z}, B_{y}, 0, \pm \frac{B_{z}}{\sqrt{\rho}}, \mp \frac{B_{y}}{\sqrt{\rho}}, 0 \right), \tag{20}$$

$$\mathbf{r}^{a} = \frac{1}{\sqrt{N}} \left( 0, 0, -B_{z}, B_{y}, 0, \pm B_{z} \sqrt{\rho}, \mp B_{y} \sqrt{\rho}, 0 \right)^{T}, \tag{21}$$

where  $N = 1/(B_y^2 + B_z^2)$  is a normalized factor and the Alfvén speed  $V_A = B_x/\sqrt{\rho}$ .

One entropy wave with:

$$\lambda^e = v_x, \tag{22}$$

$$\mathbf{l}^{e} = \left(1, 0, 0, 0, 0, 0, 0, -\frac{1}{c_{s}^{2}}\right),\tag{23}$$

$$\mathbf{r}^{e} = (1, 0, 0, 0, 0, 0, 0, 0)^{T}. \tag{24}$$

One divergence wave with:

$$\lambda^{div} = \nu_{x},\tag{25}$$

$$\mathbf{l}^{div} = (0,0,0,0,1,0,0,0), \tag{23}$$

$$\mathbf{r}^{div} = (0, 0, 0, 0, 1, 0, 0, 0)^{T}.$$
 (24)

The above described eigenvectors and eigenvalues possess singularities which can be avoided by proper normalization [6]. Then, it is relatively straightforward to apply these normalized quantities to the MHD equations.

## 5. Application of the method to magetosonic waves in a solar coronal loop

We consider the coronal plasma which is described by the ideal magnetohydrodynamic equations (13) and assume a coronal loop that is represented by an infinitely long cylinder of mass density enhancement (Fig. 1).

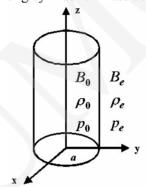


Fig. 1. A geometry of the model

The three-dimensional version of MHD equations (13) is solved numerically by using the FLASH code [7]. The high-order Riemann solver of Roe type, that is implemented in this code, yields accurate results near steep gradients and moving contact discontinuities. The MHD part is implemented with the use of Powell's method [8] which allows the divergence of magnetic field to be kept free to machine dependent round-off errors. The computer code is formally second-order accurate in space and time.

The plasma equations are solved numerically on an x-y-z Eulerian box with the dimension  $(-10,10) \times (-10,10) \times (-10,10)$ . We apply free-boundary conditions at the boundaries of the simulation region. This choice of boundary conditions is a consequence of an extension of the real medium.

MHD waves are initially present in the medium by setting the following initial condition:

$$V(r,\phi,z,t=0) = \frac{V_0}{\cosh^2\left(\frac{r}{a}\right)\cosh^2\left(\frac{z}{a}\right)},$$

$$r = \sqrt{(x^2 + y^2)},$$
(28)

where V denotes a corresponding component of the velocity and  $V_0$  is the pulse amplitude chosen as 0.005.

Including normalized variables, we measure spatial variables in units of a, time in units of the Alfvén transit time  $t_A = a/c_{Ae}$  and the perturbed mass density  $\delta \rho = \rho - \rho_0$  in units of  $\rho_0$ .

The initial profile of Eq. (28) with  $V = V_z$  excites oscillations in the perturbed mass density profile,  $\delta \rho$ , which is shown in the left panel of Fig. 2 at t = 80. As a result of the initial impact, the region above the initial pulse is compressed while the region z < 0 is rarified. These profiles are symmetric around the z-axis.

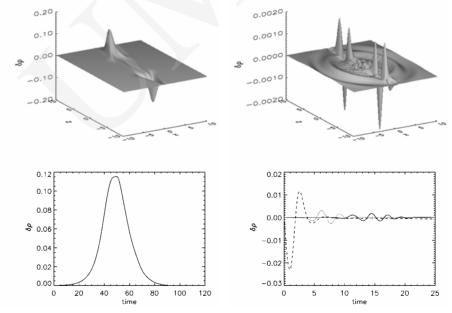


Fig. 2. The spatial profile of the perturbed mass density  $\delta\rho(x, y = 0, z, t)$  (top panels) and the time-signetures (bottom panels) which is obtained by measuring the wave signal in  $\delta\rho$  at a fixed spatial location

The above presented slow wave exhibits time-signatures which are made by collecting in time wave signals at the detection point. As the slow pulse does not

experience significant dispersive distortion, it preserves the information about the initial pulse and we choose the detection point on the loop axis at z = 4.

The right panels of Fig. 2 display a fast sausage wave. Note that the fast sausage wave exhibits short-period oscillations, the scenario of which is quite different from that in the case of the slow wave. These few-second oscillations are a result of the fact that sausage modes are more dispersive than a slow wave and the former ones are leacky for sufficiently long wavelength oscillations. As a consequence only short oscillations are guided along the coronal loop.

# 6. Summary

This paper presents a numerical model of MHD waves. This model adopts a Godunov-type method [9] which uses a Riemann solver. A computer code that is based on this method is described as being robust as it has the virtue of giving reliable results to a wide range of problems without need to be retuned. An example of applicability of this code for a highly inhomogeneous solar coronal plasma is provided.

This work was financially supported by the grant from the State Committee for Scientific Research, Republic of Poland, KBN grant no. 2 PO3D 016 25.

#### References

- [1] Priest E.R., Solar magnetohydrodynamics, Reidel Publishing Company, Dordrecht, (1982).
- [2] Murawski K., Analytical and numerical methods for wave propagation in fluids, World Scientific, Singapore, (2002).
- [3] Roe P.L., J. Comp. Phys., 43 (1981) 357.
- [4] Yee H.C., Warming R.F., Harten A., J. Comp. Phys., 57 (1985) 327.
- [5] Powell K.G., ICASE Report No., Langley, VA, 94-24 (1994).
- [6] Zachary A.L., Colella P., J. Comp. Phys., 99 (1992) 341.
- [7] Zingale M. et al., Astrophys J. Suppl., 143 (2002) 539.
- [8] Powell K.G., Roe P.L., Linde T.J., Gombosi T.I., De Zeeuw D.L., J. Comp. Phys., 154 (1999) 284
- [9] Godunov S.K., Math. Sb., 47 (1959) 271.